Particuology 115 (2026) 309–320

Contents lists available at ScienceDirect

Particuology

journal homepage: www.elsevier.com/locate/partic

DEM parameter calibration approach for cohesive ores based on PSO-BP neural network

Fangping Ye[a,b], Yanan Zhang[a], Craig Wheeler[b,c], Bin Chen[c], Chao Zhou[a], Lei Nie[a,*]

[a] Key Lab of Modern Manufacture Quality Engineering, Hubei University of Technology, Wuhan, 430068, China
[b] School of Engineering, The University of Newcastle, Callaghan, 2308, Australia
[c] TUNRA Bulk Solids, The University of Newcastle, Callaghan, 2308, Australia

HIGHLIGHTS

- A PSO-BP based DEM calibration method is proposed for cohesive lateritic nickel ore.
- Dual PSO-BP model realizes fast macro-micro mapping and parameter inversion.
- Calibration errors are below 2%, and chute flow errors are within 5%.

GRAPHICAL ABSTRACT

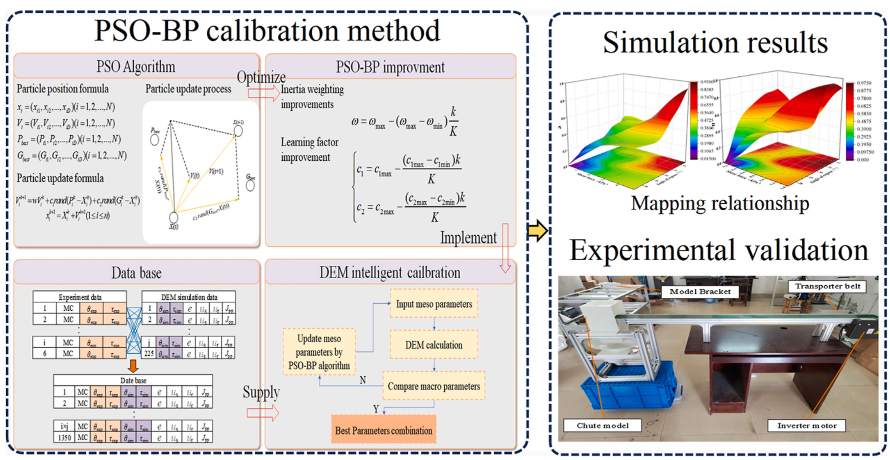

ARTICLE INFO

Keywords:
Cohesive ores
DEM parameter calibration
PSO-BP neural network
Angle of repose
Shear test

ABSTRACT

To enhance the calibration efficiency and accuracy of Discrete Element Method (DEM) parameters for cohesive bulk materials, a collaborative method integrating Particle Swarm Optimization (PSO) and Backpropagation (BP) neural networks is proposed. Key macroscopic indicators (steady-state shear stress, angle of repose) are obtained via Jenike shear and funnel tests across a 0-50% moisture range. Orthogonal experiments determine micro-parameters (e.g., static/rolling friction, surface energy) to build a macro-micro mapping database. The core of the PSO-BP dual-model lies in its collaborative mechanism: the forward BP model predicts macroscopic responses to replace time-consuming DEM simulations, while the PSO algorithm optimizes the inverse BP model to accurately infer optimal micro-parameters from experimental macro-indicators (steady-state shear stress, angle of repose). Validation shows low errors (1.14% for angle of repose, 1.63% for steady-state shear stress) and good chute flow velocity agreement. This method overcomes traditional limitations of arbitrariness and ignored parameter coupling, providing reliable support for DEM simulation and equipment design for cohesive bulk materials.

* Corresponding author.
E-mail address: leinie@hbut.edu.cn (L. Nie).

https://doi.org/10.1016/j.partic.2026.06.004
Received 16 April 2026; Received in revised form 26 May 2026; Accepted 3 June 2026
Available online 10 June 2026

1. Introduction

The application of DEM simulation in port material handling engineering and operations has expanded significantly worldwide. By simulating the behavior of granular materials, DEM enhances design optimization, improves efficiency, and reduces costs and risks, thereby generating substantial economic benefits (Ye et al., 2019). However, the accuracy of DEM simulations relies heavily on the accurate particle configuration, which requires extensive experimental data to calibrate parameters, including interparticle friction coefficients and elastic moduli. Calibration and validation are therefore essential to ensure reliable results, representing the key challenge, particularly for cohesive bulk materials (Liu et al., 2024). This study investigates lateritic nickel ore, a clay-like, weathered material composed mainly of iron, aluminum, and silicon oxides (Çoban & Baş, 2024). Its unique properties, which include strong cohesiveness (from clay minerals), high sensitivity to moisture content (MC), and irregular morphology, these characteristics distinguish it from non-cohesive particles such as sand and coal, resulting in difficulties and time-consuming calibration during DEM simulation. As an important strategic metal resource and major dry bulk cargo, its inaccurate DEM simulation causes suboptimal port equipment design, frequent clogging, and high maintenance costs. Rapid and accurate calibration of lateritic nickel ore DEM parameters enables effective prediction of its mechanical response under load, offering both scientific and practical value in the design of port bulk handling systems.

The DEM parameter calibration is the process of determining appropriate DEM parameters by continuously adjusting input parameters in the DEM model until the discrepancy between simulation results and experimental results falls within the acceptable tolerance range. Grima and Wypych (2011) calibrated the rolling friction coefficient of particles using a trial-and-error approach by comparing parameters such as bulk density, pile height, and angle of repose, achieving favorable predictive results. This method, however, fails to decouple cross-effects among cohesion, friction, and elasticity, which induces high uncertainty and is overly time-consuming when dealing with multi-moisture scenarios. Coetzee (2009; 2014) calibrated particle stiffness through compression tests, followed by sequential calibration of particle friction coefficients via shear tests or angle of repose tests. However, while this sequential calibration method reduces the degree of uncertainty in the calibration process, it also weakens the cross-effects between DEM parameters.

With advances in science and technology, neural networks have found growing application in the calibration of DEM parameters for granular materials, owing to their outstanding nonlinear fitting and learning capabilities. Benvenuti et al. (2016) trained artificial neural networks with multiple DEM simulation datasets. The trained networks focused on non-cohesive particles, ignoring cohesion and moisture. Tawadrous et al. (2010) calibrated rock micro-parameters, which differ fundamentally from clay-rich ore in cohesiveness. Long et al. (2023) proposed a recurrent neural network (RNN) -based parameter calibration model and established granular soil stress-strain sequence datasets via DEM simulations. RNN for granular soils lacks generalizability to highly cohesive, moisture-sensitive ore. Jiang et al. (2023) proposed the BP neural network-based method for calibrating DEM shear micro-parameters for granular materials. However, the initial weights and biases of BP neural networks are randomly assigned, which introduces uncertainty into the model training performance. Thus, the BP neural network is prone to being trapped in local optima and exhibits slow convergence during the training process (Tang et al., 2025). The BP neural network method is affected by random initialization, leading to susceptibility to local optima, slow convergence, and poor robustness. These flaws are salient when mapping the complex relationships between moisture, micro-parameters, and macro-strength of cohesive bulk materials like lateritic nickel ore.

Many scholars have introduced various intelligent algorithms into the field of rapid calibration of DEM micro-parameters, effectively addressing the shortcomings of traditional trial-and-error calibration methods, which are characterized by low efficiency and high subjectivity. Peng et al. (2026) optimized the SVM model using nested cross-validation and SHAP analysis, achieving high-precision calibration of rock DEM parameters. Du et al. (2025) validated the superior performance of random forests in parameter sensitivity analysis of the parallel bonding model through a comparison of various machine learning algorithms. Kholodniak et al. (2026) utilized a MLP deep learning framework to perform intelligent calibration of DEM parameters for various rock types, including granite and sedimentary rocks. Nevertheless, the above algorithms are mainly developed for rigid rock materials with stable physical properties. Given the essential differences in mechanical and physical characteristics between rock masses and cohesive ores, these data-driven methods fail to adapt to cohesive ores, whose mechanical properties and particle contact states are highly sensitive to frequent moisture content fluctuations, resulting in poor calibration stability and low prediction accuracy in practical applications.

To improve the applicability of intelligent calibration methods for ore materials, scholars have further explored targeted optimization frameworks. Wang et al. (2023) developed a deep neural network calibration method for the ore cementation particle model, significantly improving the accuracy and applicability of parameter predictions. Brandão et al. (2024) systematically reviewed the experimental determination and calibration processes of DEM input parameters, clarifying that the restitution coefficient, static friction coefficient, and rolling friction coefficient are significantly influenced by material properties, surface roughness, and particle size. Shentu and Lin (2023) proposed a two-stage machine learning framework for complex heterogeneous rock masses, which improved calibration efficiency and accuracy under conditions of multiphase and multiparameter coupling, providing a general framework for the intelligent calibration of complex DEM models. Despite the significant progress of neural networks, SVM and ensemble learning in granular material DEM calibration, current research still has prominent technical gaps that restrict the numerical simulation of cohesive ores. Existing intelligent calibration models mostly focus on materials with stable moisture characteristics and ignore the strong water sensitivity of cohesive ores; they cannot quantitatively characterize the dynamic coupling relationship between moisture content variation and DEM micro-parameters. Moreover, most conventional algorithms suffer from insufficient model interpretability and poor generalization ability under variable working conditions, and there is a lack of a specialized, adaptive calibration framework for water-fluctuating cohesive ores.

Therefore, the PSO-BP neural network-based method for DEM parameter calibration is proposed in this article. By combining the global search capability of the PSO algorithm with the nonlinear mapping strength of the BP neural network, the PSO-BP dual-model collaborative calibration system for DEM parameter calibration is established. It aims to address the issues with existing neural networks, which are prone to getting stuck in local optima, cannot adapt to cohesive materials with moisture content, and suffer from slow training convergence. The specific workflow is as follows: (1) Experimental characterization: Shear tests are conducted using the Jenike shear apparatus on lateritic nickel ore samples with varying MC to obtain the steady-state shear stress τ_{exp}. The natural angle of repose θ_{exp} is determined using the cone test. (2) Simulation database construction: DEM simulations are conducted within the parameter range specified for granular lateritic nickel ore samples, and the corresponding macroscopic response parameters (simulated angle of repose θ_{sim} and simulated shear stress τ_{sim}) are extracted. (3) Neural network model construction: The improved BP neural network based on the PSO algorithm is employed to establish both forward and inverse mapping models for DEM parameter calibration of granular lateritic nickel ore. (4) Model validation and engineering application: Inverted DEM micro-parameters derived from the inverse mapping model are employed for

DEM reconstruction simulations. Subsequently, error analyses are conducted by comparing the calibration results with experimental data (θ_{exp} and τ_{exp}). Furthermore, the effectiveness of this inverse mapping model in engineering-scale simulations is validated via comparative studies between virtual prototype simulations of the chute device and physical experiments on granular lateritic nickel ore.

2. Lateritic nickel ore calibration test

2.1. Angle of repose test

The experimental apparatus for the determination of the static angle of repose of granular lateritic nickel ore is shown in Fig. 1. The apparatus primarily consists of a supporting mounting bracket, a tray, a motor, a lead screw, a support frame, a funnel, and a speed controller. Specifically, the funnel is fixed to the mounting bracket, which is connected to the lead screw nut. The lead screw is oriented perpendicularly to the ground. First, the funnel is lowered until it comes into contact with the horizontal surface. Subsequently, the funnel is filled with 3 kg of granular lateritic nickel ore, wherein the material is uniformly distributed inside the funnel to ensure consistent discharge. Thereafter, the motor speed is regulated to actuate the upward movement of the funnel at a constant rate of 0.03 m/s. Under gravitational action, the granular material accumulates on the horizontal plane. After the accumulation has fully stabilized, the angle between the surface of the granular pile and the horizontal plane is measured, which is defined as the static angle of repose.

To eliminate subjective errors in manual measurements and improve the objectivity and accuracy of pile angle measurements, experimental images are post-processed by this article using MATLAB image processing techniques. The process is as follows in Fig. 2. Firstly, the original images undergo grayscale conversion and filtering to remove noise, eliminating interference such as uneven lighting and shadows. Then, the outer contour of the pile is extracted using the Canny algorithm. Finally, a straight line is fitted to the boundary point cloud using the least squares method, and the slope of the fitted line is taken as the tangent of the angle of repose, establishing a quantitative mapping relationship between image features and physical parameters.

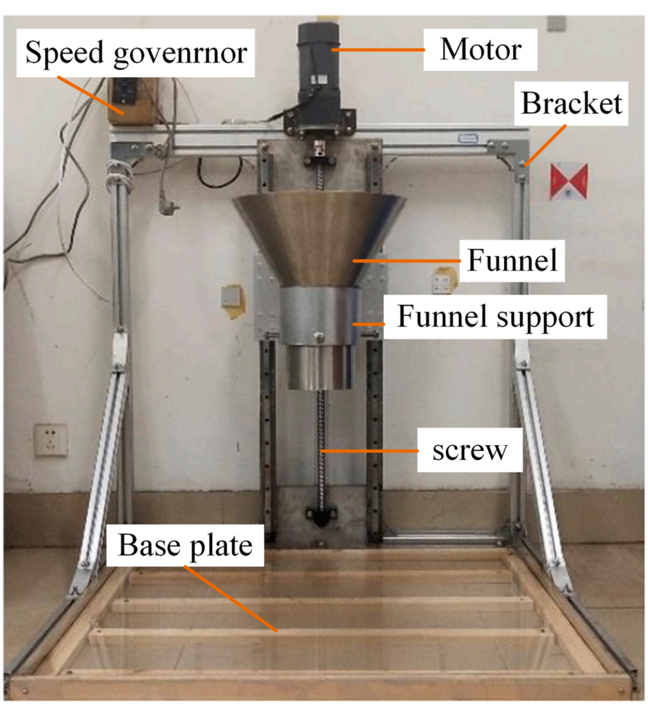

Fig. 1. Angle of repose test.

2.2. Shear test

The direct shear test is conducted using a Jenike shear tester, its equipment model is the FT-3400 powder flow behavior analyzer as illustrated in Fig. 3. The shear box features a diameter of 120 mm and a height of 30 mm. In this experiment, materials with different moisture contents are obtained by drying the raw materials and then sequentially adding water in specific mass ratios. To cover the key nodes of laterite nickel ore flow characteristics (drying, agglomeration, peak flow rate, incipient blockage and field high moisture content), moisture content gradients of 0, 10, 20, 30, 40 and 50% are adopted to better conform to experimental and industrial conditions (Liu et al., 2024; Xu et al., 2024).

The shear box is filled with particles during testing; the excess material above the shear box is leveled off, and any residual particles in the grooves are thoroughly removed. The shear rate is set at 0.3 m/s, and a vertical load of 6 kPa is applied. Test data are collected and analyzed using the powder flow behavior analyzer. Average values are calculated and adopted as the material characteristic parameters to obtain the shear property data for each MC group. The experimental data corresponding to different MC are shown in Fig. 4.

3. PSO-BP neural network algorithm

3.1. Principles of backpropagation neural networks

Based on the error BP principle, the BP neural network employs a feedforward multi-layer architecture. Its core advantage is the capacity to establish input-output mapping models for sample datasets via self-learning and data storage during extensive training, eliminating the need for explicit mathematical expressions or manual intervention in the modeling process. The self-learning mechanism of the BP neural network is based on the gradient descent algorithm, which adjusts the internal weights and biases of the network by iterative error backpropagation to minimize prediction errors. This process minimizes the sum of squared errors (SSE) of the model, thereby ensuring accurate predictions. Furthermore, in principle, the model can construct a reliable mapping between input and output variables. With sufficient sample data and when the network meets convergence criteria during training, it can be effectively utilized to predict the mechanical properties of granular materials (Jadidi et al., 2025; Liu et al., 2022). The topology of the commonly used BP neural network model is illustrated in Fig. 5, which is primarily composed of three functional layers: the input layer, the hidden layer, and the output layer.

3.2. PSO-BP neural network algorithm

The PSO algorithm is a stochastic search method inspired by the foraging behavior of bird flocks. It treats each potential solution to an optimization problem as a particle within the search space, assesses particle quality using a fitness value, and iteratively updates particle velocity and position to seek the global optimum, thereby identifying the best solution within the search space (Shami et al., 2022). The iterative formula for the velocity and position of its particles is as follows:

$$V_i^{k+1} = wV_i^k + c_1 r_1 \left(P_i^k - X_i^k\right) + c_2 r_2 \left(G_i^k - X_i^k\right) \tag{1}$$

$$X_i^{k+1} = X_i^k + V_i^{k+1} (1 \le i \le n) \tag{2}$$

where w is the inertia weight; V_i is the particle velocity, set to 0.6 in this article; c_1 and c_2 are learning factors, typically non-negative constants, set to 2.0 in this article, because when set learning factors to 2.0, neural network converges quickly during the early stages of training, and the weights exhibit only moderate oscillation near the optimal solution (Citton et al., 2025); P_i and G_i are the individual optimal position and population optimal position of the particle, respectively; X_i is the

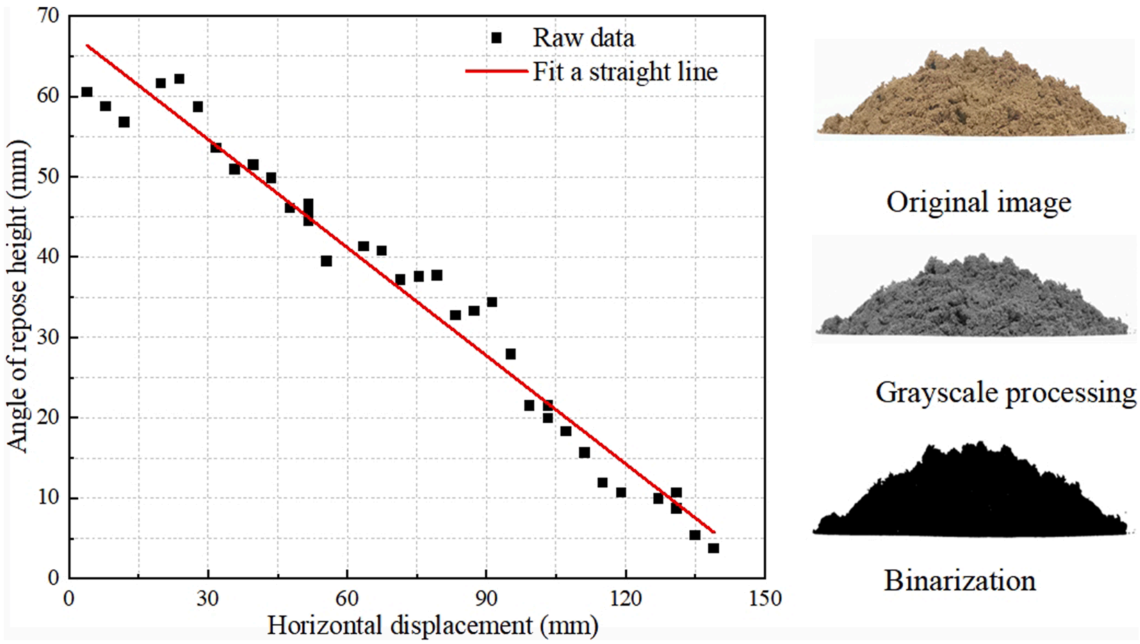

Fig. 2. Process for deriving the angle of repose.

Fig. 3. FT-3400 powder flow behavior analyzer.

position of the i-th particle.

The value of the inertia weight, w plays a crucial role in the optimization capability of the particle swarm. A larger inertia weight enhances global search, while a smaller one improves local search. To balance global and local search capabilities, a linearly decreasing inertia weight is proposed, as shown in Eq. (3):

$$w = w_{\max} - (w_{\max} - w_{\min})\frac{k}{K} \tag{3}$$

where $w_{\max}$ is the initial inertia weight (typically assigned the value of 0.9); and $w_{\min}$ is the inertia weight at the maximum number of iterations (typically assigned the value of 0.4); k is the current iteration count; K is the maximum iteration count, set to 100 in this article.

The learning factors in the algorithm govern the behavior of particles in the search space, especially their ability to follow both their own best historical positions and the global best position. In the PSO algorithm, learning factors are categorized into two types: the individual learning factor (c_1) and the social learning factor (c_2). The individual learning factor (c_1) guides the search of the particle based on its own experience. This improves the local search performance of the algorithm and facilitates the refinement of solutions. The social learning factor (c_2) governs information exchange within the swarm, thereby promoting global exploration. This mechanism helps particles escape local optima and traverse a broader region of the search space (Zou, 2021). By properly tuning these two learning factors, the PSO algorithm can effectively find the optimal solution while balancing its global and local search capabilities. This article improves the learning factor by adopting a linear time-varying approach, with the formula expressed as:

$$\begin{cases} c_1 = c_{1\ \max} - \dfrac{(c_{1\ \max} - c_{1\ \min})k}{K} \\ c_2 = c_{2\ \max} - \dfrac{(c_{2\ \max} - c_{2\ \min})k}{K} \end{cases} \tag{4}$$

where k is the current iteration count; K is the maximum iteration count, set to 100 in this article; c_1 and c_2 are learning factors, typically non-negative constants, set to 2.0 in this article.

The construction of a BP neural network mainly includes three key steps: setting the number of nodes in the input and output layers, designing the hidden layer, and normalizing the data.

(1) Based on four micro-mechanical parameters and five macro-mechanical parameters of ores samples, PSO-BP neural network models for forward modeling and inversion are established respectively. The forward modeling model takes micro-mechanical parameters as input and macro-mechanical parameters as output, while the inversion model takes macro-mechanical parameters as input and micro-mechanical parameters as output.
(2) The number of nodes in the hidden layer directly affects the model accuracy. Too many nodes tend to cause over-fitting during training, whereas too few nodes lead to under-fitting. The optimal number is calculated using the empirical formula:

$$m = \sqrt{n + l} + a \tag{5}$$

where m, n, and l represent the number of neurons in the hidden layer,

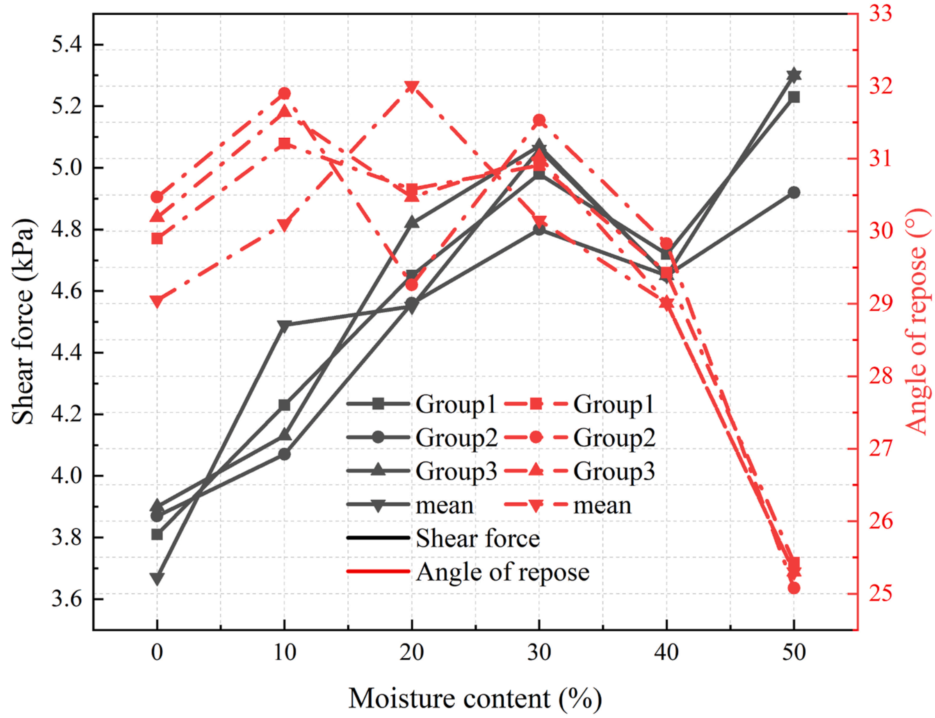

Fig. 4. Changes in angle of repose and shear stress with different moisture contents.

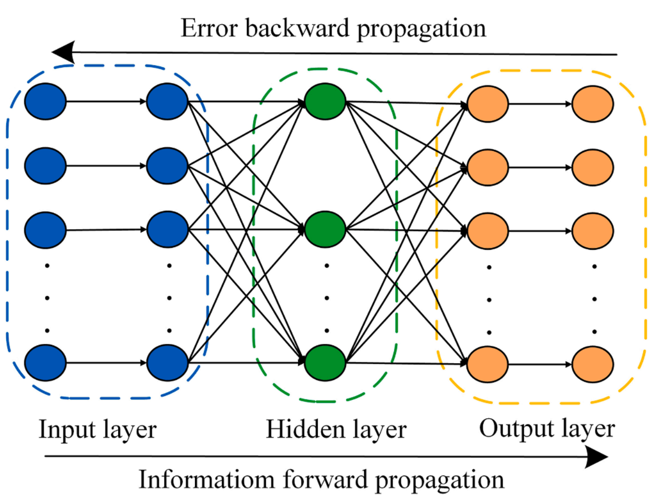

Fig. 5. Topology of the BP neural network model.

input layer, and output layer respectively, and a is a constant ranging from 0 to 10. The final number of hidden layer neurons is determined to be 10.

(3) Raw data differ in dimensions and physical meanings, so min-max normalization is adopted to scale the data to the interval [0,1] for improved training performance. The normalization formula is:

$$y = \frac{x_n - x_{\min}}{x_{\max} - x_{\min}} \tag{6}$$

where x_n is the input sample data, x_{min} and x_{max} are the minimum and maximum values of the sample data, and y is the normalized data.

After model prediction, inverse normalization is performed to restore the predicted values with real physical significance. The inverse normalization formula is given as follows:

$$x_n = y(x_{\max} - x_{\min}) + x_{\min} \tag{7}$$

Terminate neural network training when the mean squared error falls below 10^{-3}, the PSO-BP algorithm flowchart is shown in Fig. 6. The PSO-BP algorithm process is described as follows:

(1) The BP neural network is initialized; the sample data format is normalized; the total number of particle swarm weights and biases is calculated; binary encoding is conducted, and the encoded results are assigned to individual particles.
(2) PSO optimization is implemented by presetting relevant parameters and constructing the particle population, including the population size N (i.e, particle number) and the number of iterations. During particle population construction, each particle is assigned an initial random position, x_i, and velocity, v_i, for subsequent iterative processes.
(3) Calculate the fitness for each particle.
(4) Local and global optima within the particle swarm are identified and recorded.
(5) The position x_i and velocity v_i of each particle in the current swarm are updated based on fitness values, combined with the personal best position of the particle as well as the global best position of the swarm.
(6) Recalculate the fitness of each particle in the new particle swarm.
(7) The personal best positions of all particles are updated.
(8) The global optima of the particle swarm are updated.
(9) When the termination condition is satisfied, or the maximum number of allowable iterations is reached, the loop is terminated. Otherwise, the iteration count is incremented, and the process returns to Step 5.
(10) The optimal solution to the problem is output and assigned to the BP neural network.

3.3. Comparison of neural network model performance before and after improvement

Fig. 7 shows the curves of prediction accuracy error for the standard

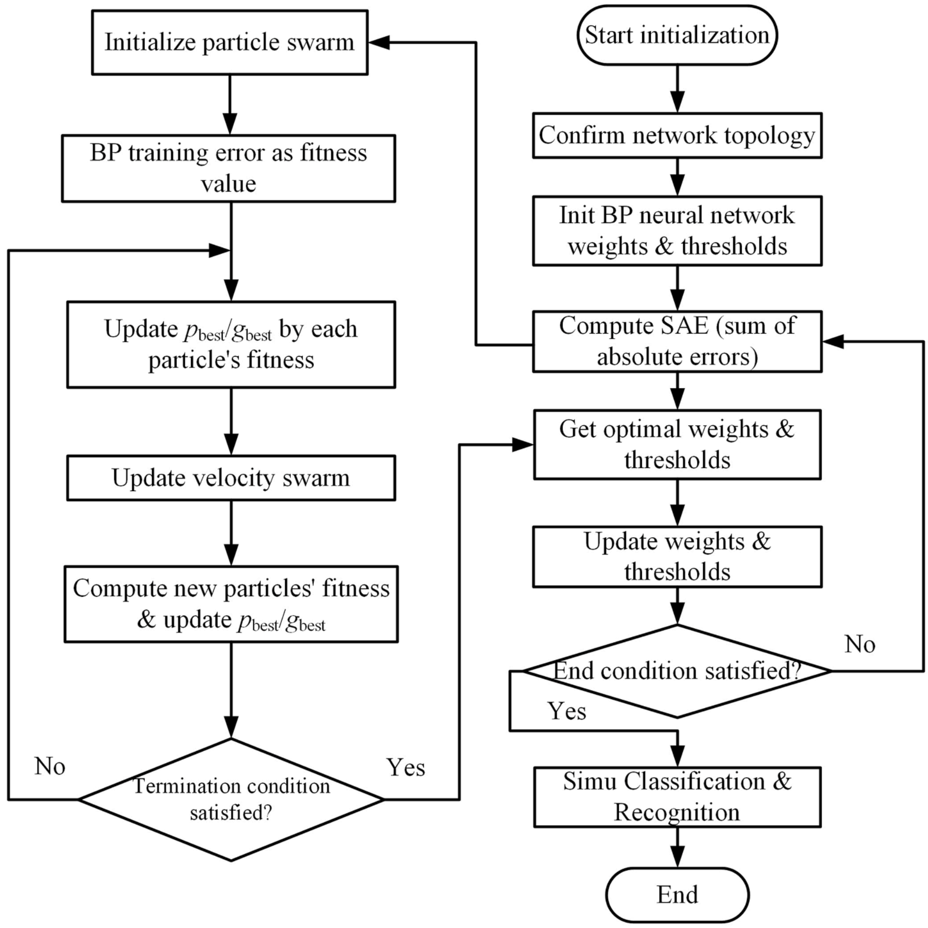

Fig. 6. Flowchart of the PSO-BP neural network algorithm.

BP neural network and the improved PSO-BP neural network when inverting and predicting macroscopic parameters of DEM under different moisture content conditions. "B" represents the standard BP neural network, and "P" represents the improved PSO-BP neural network. Overall, the prediction accuracy of the standard BP neural network is more significantly affected by changes in moisture content, exhibiting characteristics of "large fluctuations and distinct variations across ranges." In contrast, the prediction error of the improved PSO-BP neural network remains consistently at a low level, demonstrating superior stability, making it more suitable for the inversion and prediction of DEM macroscopic parameters under scenarios of dynamic moisture content fluctuations.

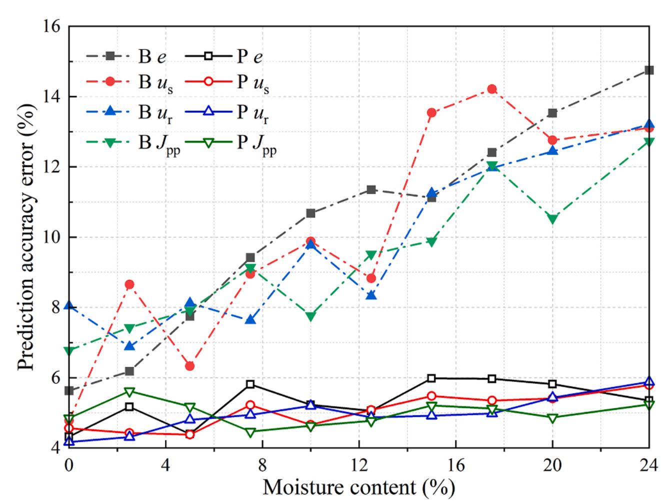

Fig. 7. Comparison of neural network prediction accuracy error before and after improvement.

4. Neural network parameter calibration

4.1. Neural network database

This article characterizes changes in moisture content by adjusting the JKR parameter (Chen et al., 2025), to accurately characterize the physical properties of lateritic nickel ore as a cohesive bulk material, this article adopts simulations using the built-in Hertz-Mindlin with JKR contact model and standard rolling friction model in EDEM software (Xu et al., 2024). The JKR model is based on Hertzian contact theory and calculates the adhesive force between particles by incorporating the concept of particle surface energy. The standard rolling friction model accounts for the rolling resistance of particles through the application of torque at the contact interface. The DEM parameters to be calibrated are the particle static friction coefficient (μ_s), rolling friction coefficient (μ_r), particle surface energy (J_{pp}), and coefficient of restitution (e). This article obtained actual particle size distribution (PSD) data through experimental testing, after particle size classification, experimental data for 1.5 mm particles are selected as the standard values for the material's macroscopic parameters. Based on data from literature on the particle-stainless steel contact of viscous moist soils (Carr et al., 2023) and the commonly used built-in material database (GEMM) of EDEM software, the parameter ranges adopted in this article are presented in detail in Table 1.

Table 1
DEM simulation parameters.

Simulation parameters	Value	Simulation parameters	Value
Particle radius	1.5 mm	Particle-particle surface energy	10~15 J m^{-2}
Poisson's ratio of particle	0.3	Particle-particle coefficient of restitution	0.15~0.75
Density of particle	2700 kg m^{-3}	Particle-particle static friction coefficient	0.2~1.0
Shear modulus of particles	5 × 10^{7} Pa	Particle-particle rolling friction coefficient	0.10~0.20
Poisson's ratio of stainless steel	0.3	Particle-stainless steel coefficient of restitution	0.48
Density of stainless steel	7800 kg m^{-3}	Particle stainless steel static friction coefficient	1.73
Shear modulus of stainless steel	7 × 10^{10} Pa	Particle-stainless steel rolling friction coefficient	0.15

Shear tests and angle of repose tests are simulated at 1:1 prototype scale using the EDEM software, ensuring spatial and topological consistency between physical experiments and numerical models. Fig. 8(a) shows the simulation test of the angle of repose test in EDEM. The funnel features a top opening with a diameter of 240 mm, a bottom cylinder (70 mm in diameter and 120 mm in height), and an overall height of 320 mm. Initially, 3 kg of lateritic nickel ore particles are loaded into the funnel, which is then lifted at a speed of 0.03 m/s to allow the particles to roll and accumulate on a 600 mm × 600 mm flat plate. After stabilization, the clipping tool in the EDEM post-processing module is used to slice the particle pile, followed by measuring the simulated angle of repose (θ_{sim}) using the Protractor tool.

Fig. 8(b) shows the simulation test of the shear test in EDEM. During the shear test simulation, a constant pressure of 6.0 kPa is applied to the clipping cover along the vertical direction. Once the material particle simulation process stabilizes, a constant pressure is maintained on the clipping cover, while a rotational shear rate of 0.48 rpm is applied to the shear box. The simulation calculation yields the steady-state shear stress τ_{sim}. In this model, the gravitational parameter g is set to 9.81 m/s^2 to ensure the physical authenticity of the dynamic response characteristics of the particle system.

An orthogonal experimental design is employed to construct 225 parameter combinations for four parameters: coefficient of restitution, particle static friction coefficient, particle dynamic friction coefficient, and interparticle surface energy in this article. From the total of 450 DEM simulations, a comprehensive parameter database containing 450 sets of angle of repose and shear force response data is established. By pairing the experimental data from six MC conditions (0-50% by mass) in Fig. 4 with corresponding simulation data, a total of 1350 sets of paired experimental-simulation data are obtained (6×225). The database design approach is shown in Fig. 9.

4.2. Neural network test results

A three-channel data partitioning mechanism is employed to construct an anti-overfitting data architecture with 70% training set, 15% validation set and 15% test set (Liu et al., 2024), thereby establishing a bidirectional parameter correlation model in this article. The forward model takes the micro-parameter vector $X = \{\mu_s, \mu_r, J_{pp}, e\}$ as

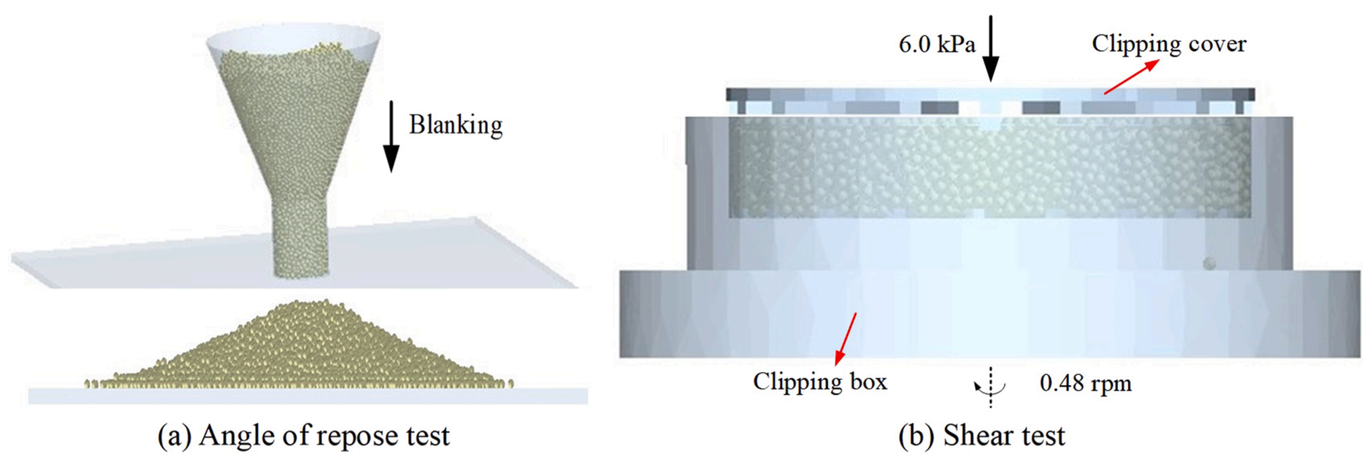

Fig. 8. Angle of repose test and shear test simulation model.

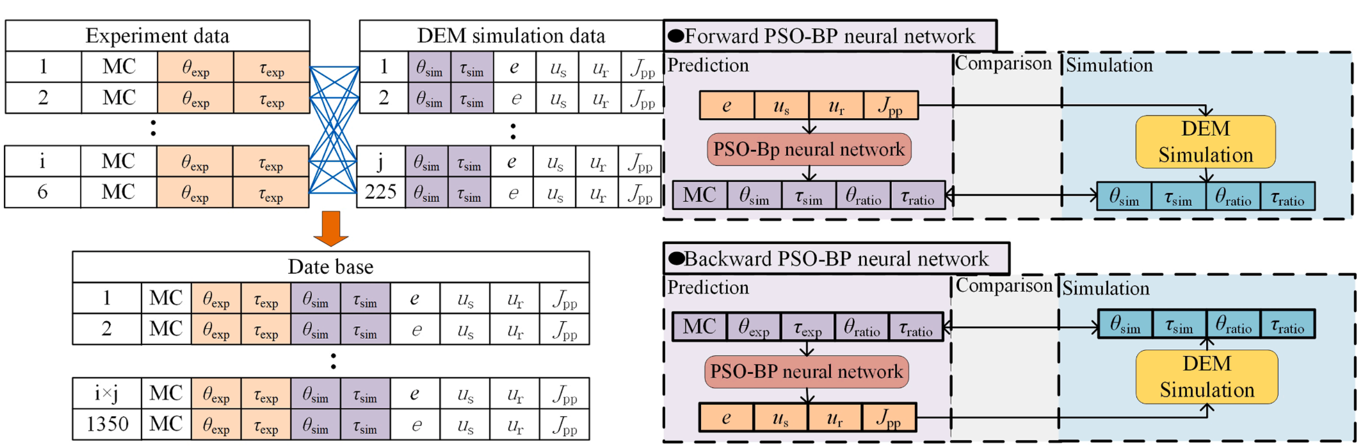

Fig. 9. DEM simulation database.

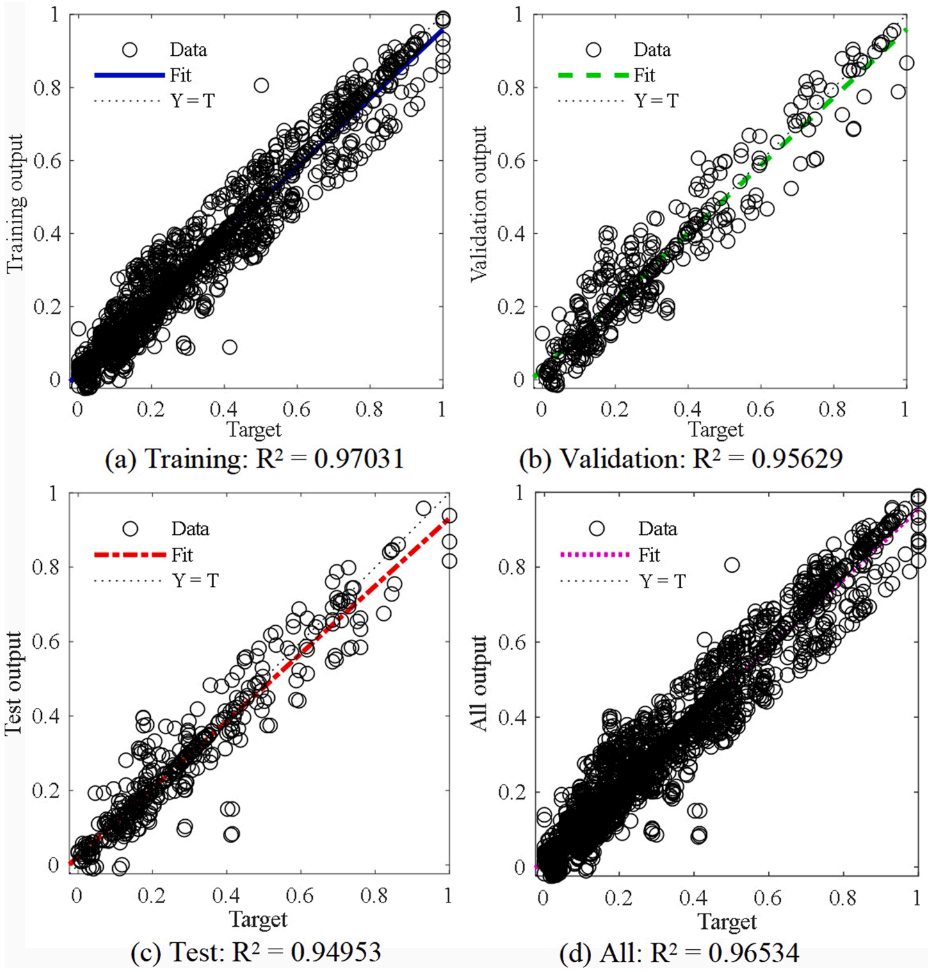

Fig. 10. Training effect diagram of forward PSO-BP neural network.

input and outputs the macro-parameter vector $Y = \{MC, \theta_{\mathrm{sim}}, \tau_{\mathrm{sim}}, \theta_{\mathrm{ratio}}, \tau_{\mathrm{ratio}}\}$ to construct a surrogate model for DEM simulation (where $\theta_{\mathrm{ratio}} = \theta_{\mathrm{sim}}/\theta_{\mathrm{exp}}$, $\tau_{\mathrm{ratio}} = \tau_{\mathrm{sim}}/\tau_{\mathrm{exp}}$). The parameter inversion mechanism is employed by the inverse model, with the macro-parameter vector Y adopted as the input to invert the micro-parameter vector X. The forward PSO-BP model consists of a four-node input layer, five-node output layer, and a single ten-node hidden layer, as shown in Fig. 10.

During the training phase, the model achieves an R^2 value of 0.97, followed by $R^2 = 0.95$ in the validation phase and $R^2 = 0.95$ in the testing phase. The regression coefficients across all three phases exceeded the 0.9 threshold, validating the generalization capability of the network architecture.

The inverse PSO-BP model comprises a five-node input layer, a four-node output layer, and a single ten-node hidden layer. Fig. 11 illustrates the performance of the model across training, validation, and test datasets, with regression coefficients exceeding the 0.8 significance threshold in all stages. This indicates that the trained model achieves a good fit between predictions and actual results. The inverse mapping model can accurately reconstruct DEM micro-parameters, meeting the accuracy requirements for DEM parameter calibration.

Fig. 12 illustrates the fit between the neural network-predicted microscopic parameters (including the static friction coefficient between particles μ_s, the rolling friction coefficient between particles μ_r, the interfacial energy between particles J_{pp}, and the coefficient of restitution between particles e) and the actual values under 100 sample sets. The root mean square error (RMSE) for each parameter is less than 0.1, indicating that the deviation between the model's predictions and the actual values from the DEM simulation is small, demonstrating high goodness of fit and prediction accuracy. Thus, the DEM macro-micro parameter inversion model based on the PSO-BP neural network can effectively and accurately identify micro-mechanical parameters. This model enables rapid inversion of micro-parameters based on macro-mechanical parameters, significantly reducing the time required for micro-parameter calibration in DEM numerical simulations and thereby enhancing the overall efficiency of macro-micro parameter correlation studies.

Fig. 13 illustrates the relationship between the angle of repose of the lateritic nickel ore, steady-state shear strength (which is derived from the PSO-BP inverse neural network prediction model) and the microscopic parameters of the lateritic nickel ore (μ_s, μ_r, J_{pp}, e). The prediction results reveal a complex nonlinear relationship among the angle of repose, shear strength and DEM parameters, indicating that the macroscopic flow behavior of particles results from the synergistic interaction of multiple DEM parameters.

Analysis of Fig. 13 reveals that the coefficient of restitution e exhibits a nonlinear response to macroscopic parameters, characterized by a weak response in the low range and a strong enhancement in the high range. The influence of the static friction coefficient μ_s between particles on macro parameters exhibits a nonlinear pattern characterized by a gradual increase in the low range, a steep increase in the medium-to-high range, and a gradual decrease in the high range. The influence of the kinetic friction coefficient μ_r between particles on macro parameters exhibits a unimodal nonlinear pattern. The influence of the interparticle surface energy J_{pp} on macro parameters exhibits a nonlinear pattern characterized by a weak response in the low range and a strong enhancement in the high range.

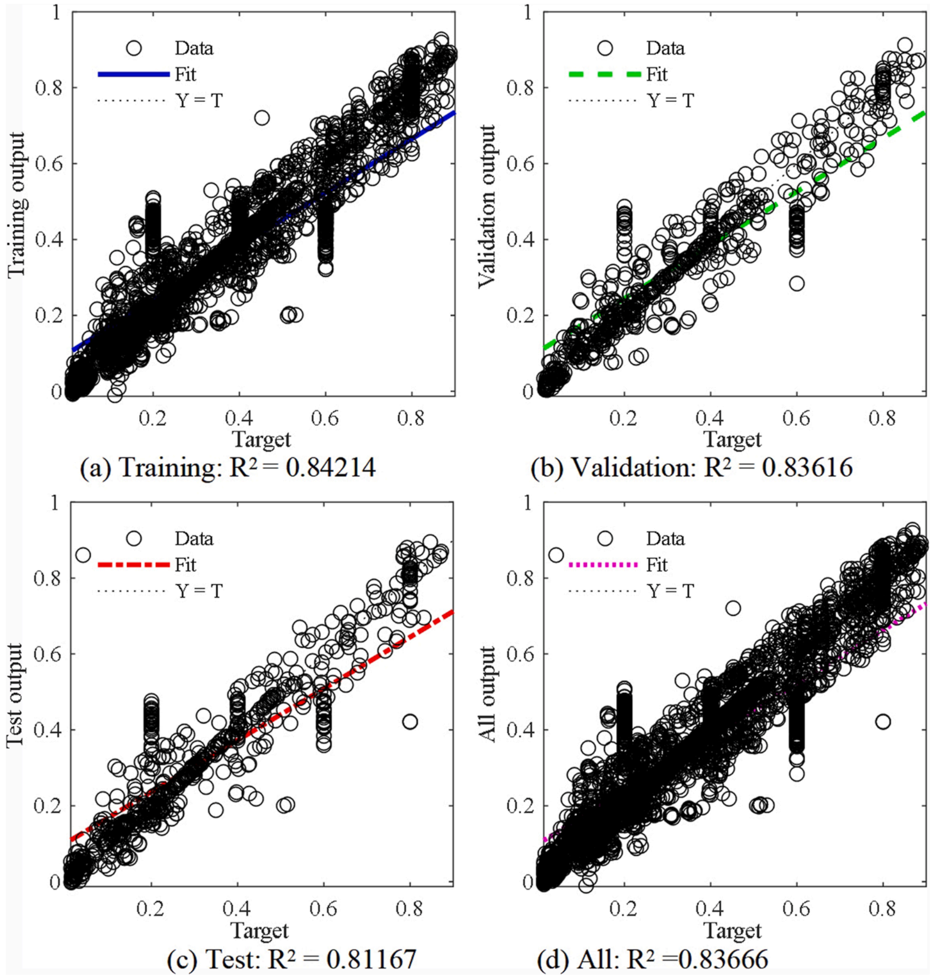

Fig. 11. Training results of the backward PSO-BP neural network.

4.3. Analysis of reverse validation results

Based on the output values from the reverse neural network, simulation tests are conducted on the angle of repose and shear behavior of lateritic nickel ore. Under 40% moisture content (MC) conditions, steady-state shear stress (τ_{exp}) and angle of repose (θ_{exp}) are measured for laterite nickel ore samples. These values are used to obtain inverted micro-parameters, which are then applied to DEM reconstruction simulations, yielding simulated steady-state shear stress (τ_{sim}) and simulated angle of repose (θ_{sim}). The results are compared as shown in Fig. 14.

Simulation and field test results indicate that there are no significant differences in the particle shape and related parameters of laterite nickel ore. Four repeated simulation tests of the angle of repose yielded values of 31.0°, 31.4°, 30.5°, and 30.9°, with a mean of 30.95° and a standard deviation of 0.32°. The relative error compared to the measured angle of repose (with the measured value serving as the reference standard) is only 1.14%. Four repeated simulated shear tests yield steady-state shear strengths of 4.33, 4.51, 4.23, and 4.37 kPa, with a mean of 4.36 kPa and a standard deviation of 0.12 kPa. The relative error relative to the measured steady-state shear strength (with the latter as the reference standard) is only 1.63%. The results demonstrate that the PSO-BP neural network method is feasible for inverting simulated physical parameters of lateritic nickel ore particles.

5. Flow test validation for chutes

To verify whether this model can accurately reflect the physical and mechanical properties of lateritic nickel ore, and to distinguish between the angle of repose tests and shear tests, validation experiments are carried out. The validation work combines chute flow tests with corresponding DEM simulations. The velocity of the material exiting the discharge port is used as the response value. Measured values are compared with simulated values, and the relative error is employed to assess the accuracy of the DEM simulation model.

Based on the actual transfer chute drawings collected from the port site, a three-dimensional model of the chute is constructed. This model is then scaled down proportionally for 3D printing, as shown in Fig. 15. Lateritic nickel ore with a MC range of 0-50% is selected. Each group underwent four parallel tests, with a total material mass of 5 kg per test. The conveyor belt speed is set at 2 m/s for the experiments. Before the test begins, the material on the conveyor belt, is evenly distributed incorporating white round pebble particles into the material. During the test, feed material onto the conveyor belt continuously. A high-speed camera at the chute discharge outlet is used to record the discharge process. After the test concludes, the high-speed camera footage is analyzed to track the displacement distance of individual white pebbles within a specific time interval following their exit from the chute. The material movement over short distances are treated as approximately uniform motion. The positions of individual pebbles are recorded at different time points to calculate the material flow velocity at the chute outlet, v_{exp}.

The positions of the particles with different moisture contents are shown in Fig. 15. The flow velocity of the particles within the chute is determined based on the displacement distance recorded over 0.1 s. The forces between particles in lateritic nickel ore vary with moisture

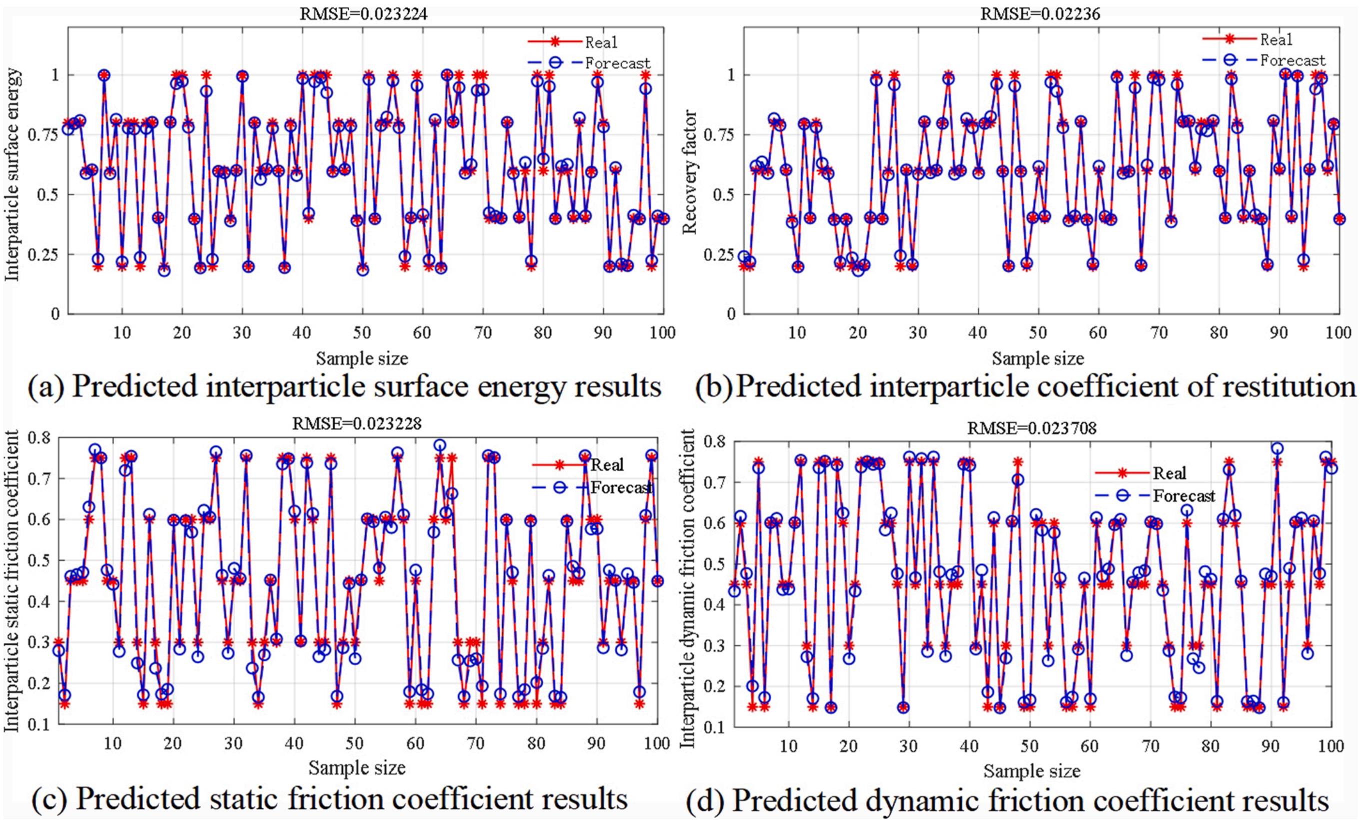

Fig. 12. Prediction results of the reverse PSO-BP neural network.

content, resulting in different flow rates. As illustrated in Fig. 15, the flow velocity decreases gradually from 1.96 m/s at 0% MC to 1.84, 1.58, 1.36, 1.22 and 1.16 m/s under MC values of 10%, 20%, 30%, 40% and 50%, respectively.

The three-dimensional chute model is imported into EDEM software. The material of the experimental apparatus is PLA (polylactic acid) with intrinsic parameters: density 1.17×10^3 kg/m^3, Poisson's ratio 0.33, shear modulus 9.89×10^5 kPa. Lateritic nickel ore with 0-50% MC is selected to derive micro-parameters for DEM reconstruction simulation. Four parallel flow simulations are conducted to obtain the simulated flow velocity v_{sim}. The mean value of the four parallel test results is recorded as the simulation outcome, as shown in Table 2.

The DEM simulation parameters for cohesive lateritic nickel ores are calibrated using DEM simulation software. Calibration is performed based on the JKR contact model and utilizing the micro-parameters inverted via the reverse PSO-BP neural network algorithm. The relative error between the simulated and measured flow velocities at the chute outlet is within 5%, and the physical and mechanical properties of the simulated lateritic nickel ore align with the actual lateritic nickel ore characteristics. This demonstrates that the method for calibrating DEM simulation parameters for cohesive lateritic nickel ore clay soil is accurate and feasible.

6. Conclusions

This study combines field experiments and DEM simulations based on angle of repose and shear tests of lateritic nickel ore. Key parameters are calibrated in EDEM. Using the two indicators as response variables, forward and inverse PSO-BP models are established in MATLAB. The forward model replaces time-consuming DEM computations, and the inverse model is used to determine DEM micro-parameters. The main conclusions of this article are presented as follows:

(1) The DEM parameter calibration framework for cohesive lateritic nickel ore is proposed using a PSO-BP neural network. Steady-state shear stress and angle of repose under 0-50% moisture content are tested to provide reliable macroscopic benchmarks.
(2) The dual PSO-BP model is developed: the forward model predicts macro responses to replace repeated DEM simulations, and the inverse model identifies micro-parameters efficiently. PSO optimization improves the convergence and accuracy of the BP network.
(3) Validations show that the prediction errors of angle of repose and shear stress are 1.14% and 1.63%, and chute flow errors are within 5%. The method avoids subjective calibration and improves DEM simulation reliability for port bulk handling equipment design.
(4) This study mainly adopts angle of repose and steady-state shear strength as response indicators. Future work will introduce more indicators (e.g., particle breakage rate and flow uniformity) to establish a multi-objective optimization calibration model, to support multi-performance collaborative optimization in engineering simulations.

CRediT authorship contribution statement

Fangping Ye: Methodology, Investigation, Conceptualization. **Yanan Zhang:** Writing – original draft, Software. **Craig Wheeler:** Writing – review & editing, Resources. **Bin Chen:** Writing – review & editing, Methodology. **Chao Zhou:** Validation, Data curation. **Lei Nie:** Supervision, Funding acquisition.

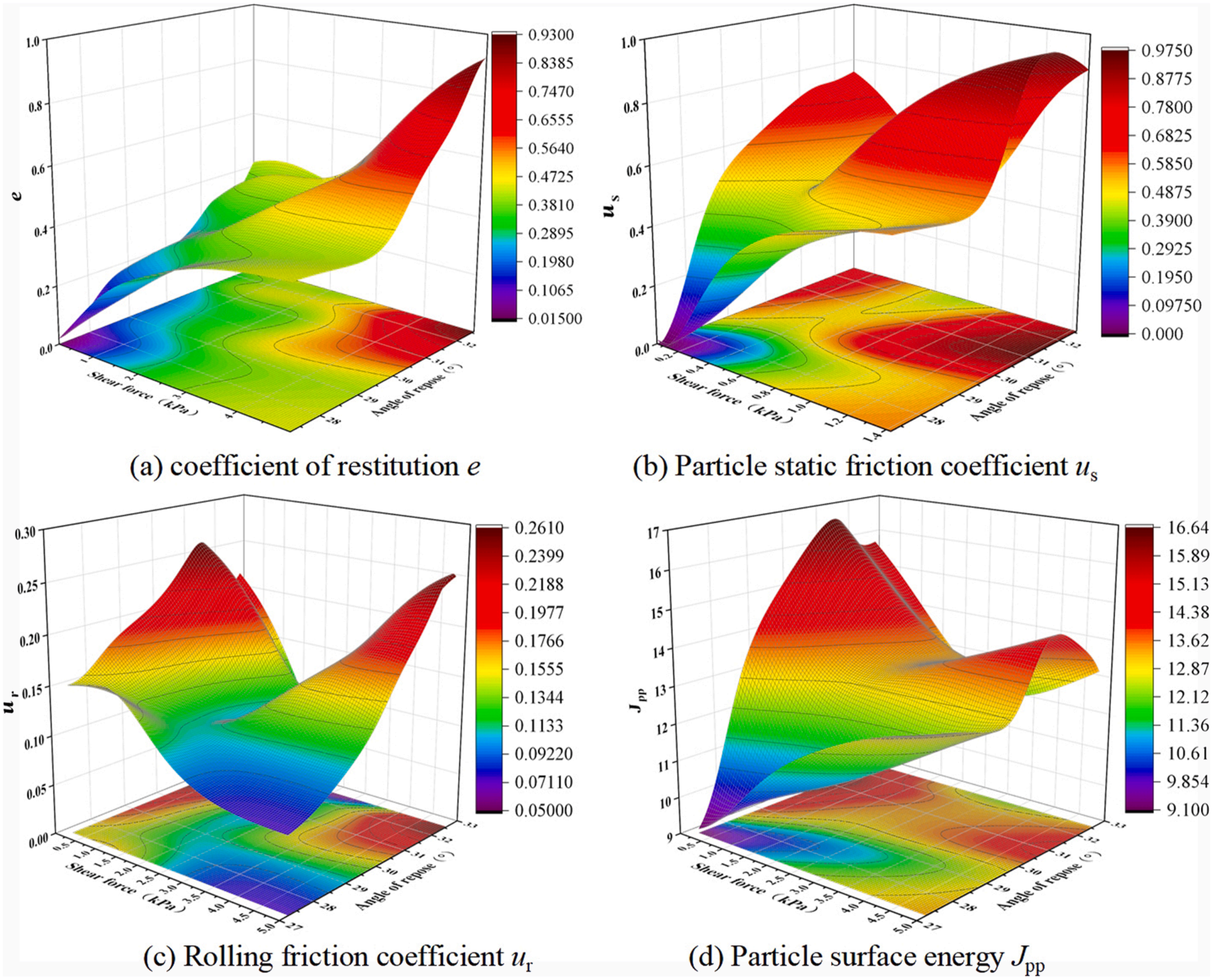

Fig. 13. Cloud map of interactions among parameters in the neural network.

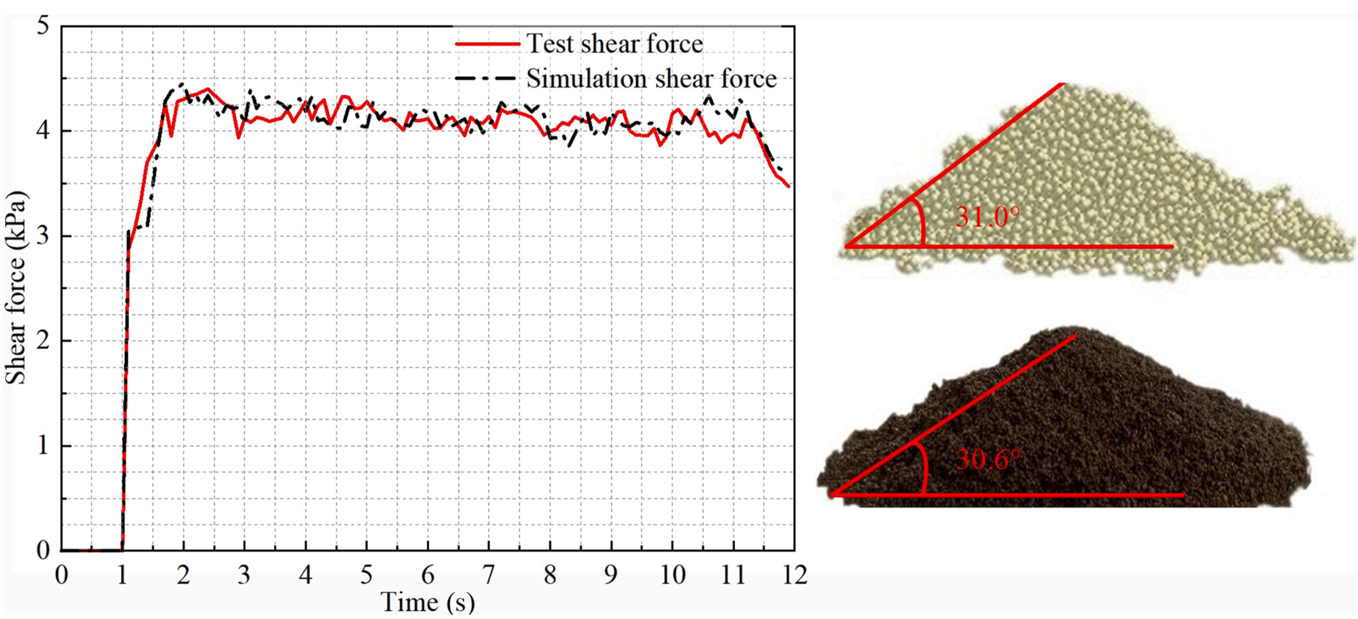

Fig. 14. Comparison of shear test results and accumulation test results.

Fig. 15. Flow chute experiment and results.

Table 2
Flume flow velocity test data for nickel ore soil at different MC levels.

MC (%)	Simulated value (m s^{-1})	Test value (m s^{-1})	Relative error (%)
0	1.90	1.96	3.06
10	1.75	1.84	4.89
20	1.65	1.58	4.43
30	1.30	1.36	4.41
40	1.16	1.22	4.92
50	1.13	1.16	2.59

Declaration of competing interest

The authors declare that they have no known competing financial interests or personal relationships that could have appeared to influence the work reported in this paper.

Acknowledgment

This work was supported by International Science and Technology Joint Research Project of Hubei, China (grant No. 2024EHA007).

References

Benvenuti, L., Kloss, C., & Pirker, S. (2016). Identification of DEM simulation parameters by artificial neural networks and bulk experiments. *Powder Technology, 291*, 456–465.

Brandão, R. J., Calheiros, C. J. P., Machado, M. V. C., Lima, R. M., Duarte, C. R., & Barrozo, M. A. S. (2024). A systematic evaluation of DEM input parameters measurement and calibration. *Powder Technology, 448*, Article 120157.

Carr, M. J., Roessler, T., & Robinson, P. W. (2023). Calibration procedure of discrete element method (DEM) parameters for wet and sticky bulk materials. *Powder Technology, 429*, Article 118919.

Chen, F., Yang, L., Cui, T., Zhang, D., He, X., & Zhang, K. (2025). Establishment and parameter calibration of the discrete element model for typical clay in hilly and mountainous areas. *International Journal of Agricultural and Biological Engineering, 18*, 26–38.

Citton, O. C., Richert, F., & Biehl, M. (2025). The role of the learning rate in layered neural networks with ReLU activation function. *Proceedings of the 33rd European symposium on artificial neural networks, computational intelligence and machine learning (ESANN 2025)* (pp. 437–442).

Çoban, B., & Baş, A. D. (2024). HPAL of a lateritic nickel ore: An investigation on the relationship between nickel and cobalt extraction and acid consumption. *Minerals Engineering, 218*, Article 109014.

Coetzee, C. J. (2009). Calibration of granular material parameters for DEM modelling and numerical verification by blade-granular material interaction. *Journal of Terramechanics, 46*, 15–26.

Coetzee, C. J., & Nel, R. G. (2014). Calibration of discrete element properties and the modelling of packed rock beds. *Powder Technology, 264*, 332–342.

Du, X., Liu, W., Peng, C., et al. (2025). Study on micro-parameters of parallel bond model based on machine learning algorithm. *Computational Particle Mechanics, 12*, 2637–2654.

Grima, A. P., & Wypych, P. W. (2011). Investigation into calibration of discrete element model parameters for scale-up and validation of particle-structure interactions under impact conditions. *Powder Technology, 212*, 198–209.

Jadidi, B., Ebrahimi, M., Ein-Mozaffari, F., & Lohi, A. (2025). Calibration of DEM input parameters for simulation of the cohesive materials: Comparison of response surface method and machine learning models. *Particuology, 103*, 1–17.

Jiang, W., Tan, Y., Yan, J., et al. (2023). A BP neural network-based micro particle parameters calibration and an energy criterion for the application of strength reduction method in MatDEM to evaluate 3D slope stability. *Revista Internacional de Métodos Numéricos para Cálculo y Diseño en Ingeniería, 39*, 12–23.

Kholodniak, M., Panchenko, A., & Berinskii, I. (2026). On deep learning calibration for DEM simulation of sedimentary and igneous rocks. *Powder Technology, 470*, Article 121929.

Liu, Y., Wang, L., Gu, K., & Liu, M. (2022). Artificial neural network (ANN)-Bayesian probability framework (BPF) based method of dynamic force reconstruction under multi-source uncertainties. *Knowledge-Based Systems, 237*, Article 107796.

Liu, Z., Yuan, J., Shen, J., Hu, Y., & Chen, S. (2024). A new DEM calibration method for wet and stick materials based on the BP neural network. *Powder Technology, 448*, Article 120228.

Long, S., Xu, S., & Zhang, Y. (2023). Method of soil-elastoplastic DEM parameter calibration based on recurrent neural network. *Powder Technology, 416*, Article 118222.

Peng, C., Xiang, S., Liu, W., Wang, X., Li, B., & Wu, S. (2026). Prediction of compressive strength and calibration of mesoscopic parameters of particle discrete element model based on explainable machine learning. *Powder Technology, 476*, Article 122427.

Shami, T. M., El-Saleh, A., A, & Alswaitti, M. (2022). Particle swarm optimization: A comprehensive survey. *IEEE Access, 10*, 10031–10061.

Shentu, J., & Lin, B. (2023). A novel machine learning framework for efficient calibration of complex DEM model: A case study of a conglomerate sample. *Engineering Fracture Mechanics, 279*, Article 109044.

Tang, G., Lei, J., Du, H., Yao, B., Zhu, W., & Hu, X. (2025). Proportional-integral-derivative controller optimization by particle swarm optimization and back propagation neural network for a parallel stabilized platform in marine operations. *Journal of Ocean Engineering and Science, 10*, 1–10.

Tawadrous, A. S., DeGagné, D., & Pierce, M. (2010). Prediction of uniaxial compression PFC3D model micro-properties using artificial neural networks. *International Journal for Numerical and Analytical Methods in Geomechanics, 33*, 1953–1962.

Wang, Y., Wang, G., Wu, S., Liu, Z. B., & Fang, Y. (2023). A calibration method for ore bonded particle model based on deep learning neural network. *Powder Technology, 420*, Article 118417.

Xu, N., Tang, S., Lin, D., Geng, R., Wang, R., & Liang, X. (2024). Complex granular flows of sticky-wet material on flip-flow screens: Calibration of discrete element simulations. *Particuology, 84*, 290–308.

Ye, F., Wheeler, C., Chen, B., Hu, J., Chen, K., & Chen, W. (2019). Calibration and verification of DEM parameters for dynamic particle flow conditions using a backpropagation neural network. *Advanced Powder Technology, 30*, 292–301.

Zou, X. (2021). Analysis of consumer online resale behavior measurement based on machine learning and BP neural network. *Journal of Intelligent & Fuzzy Systems, 40*, 2121–2132.